JVST A
Journal of Vacuum Science & Technology A

Optical dielectric properties of HfO_2-based films

Cite as: J. Vac. Sci. Technol. A **40**, 033412 (2022); https://doi.org/10.1116/6.0001651
Submitted: 24 November 2021 • Accepted: 08 April 2022 • Published Online: 28 April 2022

Hongyi Dou, **Nives Strkalj, Yizhi Zhang, et al.**

JVST A
Journal of Vacuum Science & Technology A

ARTICLE

avs.scitation.org/journal/jva

Optical dielectric properties of HfO_2-based films

Cite as: J. Vac. Sci. Technol. A 40, 033412 (2022); doi: 10.1116/6.0001651
Submitted: 24 November 2021 · Accepted: 8 April 2022 ·
Published Online: 28 April 2022

Hongyi Dou,[1] Nives Strkalj,[2] Yizhi Zhang,[1] Judith L. MacManus-Driscoll,[2,a)] Quanxi Jia,[3,b)] and Haiyan Wang[1,4,c)]

AFFILIATIONS

[1]School of Materials Engineering, Purdue University, West Lafayette, Indiana 47907
[2]Department of Materials Science and Metallurgy, University of Cambridge, 27 Charles Babbage Road, Cambridge CB3 0FS, United Kingdom
[3]Department of Materials Design and Innovation, University at Buffalo, the State University of New York, Buffalo, New York 14260
[4]School of Electrical and Computer Engineering, Purdue University, West Lafayette, Indiana 47907

Note: This paper is a part of the Special Collection Honoring Dr. Scott Chambers' 70th Birthday and His Leadership in the Science and Technology of Oxide Thin Films.

[a)]**Electronic mail:** jld35@cam.ac.uk
[b)]**Electronic mail:** qxjia@buffalo.edu
[c)]**Author to whom correspondence should be addressed:** hwang00@purdue.edu

ABSTRACT

We report the dielectric Properties of HfO_2-based films in the optical–high frequency range. The demonstrated tunability of the optical dielectric constant of HfO_2-based compounds is of great relevance for optoelectronic applications, e.g., high-refractive index dielectrics for nanoantenna and optical coatings for electronic displays. Since the optical dielectric constant of HfO_2 is determined by the electronic structure and its crystal environment, we tune the physical properties of HfO_2 films on MgO by adding different dopants. In this work, we aim to determine the influence of doping together with the resulting crystal structure on the optical dielectric constant. Hence, we studied 20 mol. % Y-doped HfO_2 (HYO), $Hf_{0.5}Zr_{0.5}O_2$ (HZO), and $Hf_{0.5}Ce_{0.5}O_2$ (HCO). Among the dopants, Y_2O_3 has the lowest, ZrO_2 an intermediate, and CeO_2 the highest real part of the optical dielectric constant. The optical dielectric constant is found to be lowest in the cubic HYO films. An intermediate dielectric constant is found in HZO films that is predominantly in the monoclinic phase, but additionally hosts the cubic phase. The highest dielectric constant is observed in HCO films that are predominantly in the cubic phase with inclusions of the monoclinic phase. The observed trend is in good agreement with the dominant role of the dopant type in setting the optical dielectric constant.

I. INTRODUCTION

Beyond the use of HfO_2 as a high-k dielectric material in the semiconductor industry,[1–4] the recent discovery of ferroelectricity and resistive switching in HfO_2 and its compounds opens the use of this material system for further applications in microelectronics.[5–9] Compounds based on HfO_2, including Y-doped HfO_2 (HYO), Zr-doped HfO_2 (HZO), and Ce-doped HfO_2 (HCO), have drawn increasing attention in recent years because of the possibility to control the crystal structure and thus improve the electrical properties of HfO_2.[10–16] There are only a few studies on the optical response of the HfO_2-based films at higher frequencies relevant for optical applications.[17–19] Despite the opportunity to use doping to tailor the refractive index, which is an important property in determining the focusing power of lenses and the light-guiding nature of optical fibers, the characterization of solid solutions of HfO_2-based compounds is still largely missing.

In this paper, we evaluate the dielectric constant of HfO_2-based films of selected compounds on MgO (001) substrates. The structures of these films are characterized using x-ray diffraction (XRD) and transmission electron microscopy (TEM). We find that the 20 mol. % Y-doped HfO_2 (HYO) film stabilizes in the cubic phase, the $Hf_{0.5}Zr_{0.5}O_2$ (HZO) film stabilizes predominantly in the monoclinic phase with regions in the cubic phase, and the $Hf_{0.5}Ce_{0.5}O_2$ (HCO) film stabilizes predominantly in the cubic phase with regions in the monoclinic phase. We discuss the roles of phase change under doping and refractive index of a solid solution individually for each film to account for our observations. The

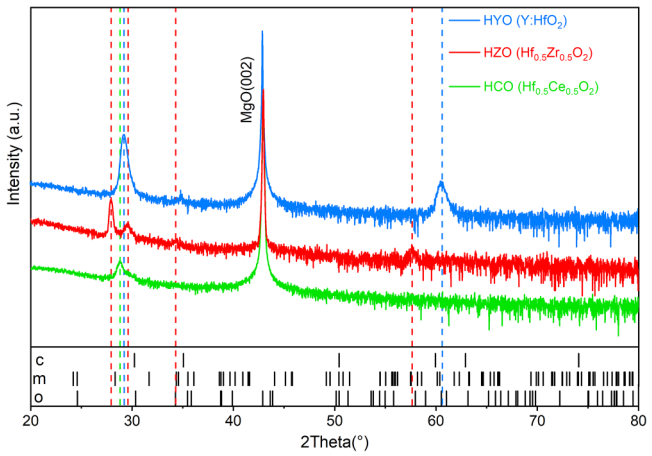

FIG. 1. XRD Θ-2Θ scan of HYO (Y:HfO_2), HCO ($Hf_{0.5}Ce_{0.5}O_2$), and HZO ($Hf_{0.5}Zr_{0.5}O_2$). The reference peak positions of the cubic (c)/monoclinic (m)/orthorhombic (o) phases of HfO_2 are provided on the bottom of the plot.

optical dielectric constant is found here to be the lowest in HYO films, intermediate in HZO films, and highest in HCO films. The dielectric constant is found to be higher in films doped with material of a higher dielectric constant. Our findings show that the dielectric constant can be tuned by incorporating constituent materials with different dielectric constants, which is of interest in optoelectronic devices.

II. EXPERIMENT

Films of HYO, HZO, and HCO were deposited on (001)-oriented MgO substrates via pulsed laser deposition (PLD) using a KrF excimer laser (λ = 248 nm) operating at a repetition rate of 5 Hz. The MgO substrate was chosen because of its low dielectric constant to minimize the complexity in optical analysis.[20] A substrate temperature of 800 °C, oxygen pressure of 25 mTorr, and laser fluence of 1 J/cm^2 were used during deposition. After deposition, the films were cooled in an oxygen atmosphere of 200 Torr without any further *in situ* thermal treatment. The structural characterization of all three films was done by x-ray diffraction (XRD) and transmission electron microscopy (TEM). The thickness of our films is determined as an average value of ten points across each film measured from TEM. Optical responses of the samples were measured using a J. A. Woollam VASE ellipsometer and further analyzed using the CompleteEASE software from the same company.

III. RESULTS

We first characterize the structure of the samples using XRD, see Fig. 1. For the HYO film, only the diffraction peaks (111) and (222) of the cubic phase are observed in the Θ-2Θ scan. For the HZO and HCO films, several additional peaks appear in the Θ-2Θ scan, which suggests incorporation of additional phases in the film such as the orthorhombic and cubic phase in HZO, and cubic phase in HCO. The peak positions of our HfO_2-based solid solutions differ with respect to HfO_2 in peak positions in XRD because of the different ionic radii of dopant materials, as shown in Table I. The XRD pattern of HfO_2 is expected to best match with the XRD pattern for the HZO films because of the similar ionic radius and smaller crystallite size. Both Y^{3+} ions and Ce^{4+} ions are about 25% larger than the Hf^{4+} and Zr^{4+} ions. Doping with either Y_2O_3 or CeO_2 is thus expected to result in an increase in lattice parameters of HfO_2 and thus a downward shift of 2Θ values. Besides the larger lattice parameter of Y_2O_3 and the larger Y^{3+} ions, the smaller coordination number of Y^{3+} cations induces oxygen vacancies and therefore introduces more complexity to the consequent refractive index. The change in the electron density as a result of the charge compensation for the incorporation of oxygen vacancies and also the phase changes are all possible contributing factors to the aforementioned complexity. The discrepancy to the pure HfO_2 for our films is expected to be smaller for HYO than for HCO because of the smaller amount of the Y dopant with respect to Ce dopant.

Since the XRD analysis is complex as described above, we have used the TEM technique to make final conclusions on the phase composition. The diffraction patterns and local fast Fourier transforms (FFT) captured in the microscopic images provide more information about crystal planes other than the out-of-plane directions. For the HYO film, the thickness is found to be 84 ± 2 nm. The textured growth of HYO on top of the MgO substrate is further confirmed by the sharp interface between HYO and MgO, as shown in Figs. 2(a) and 2(b). Electron diffraction shown in Fig. 2(c) further confirms the stabilization of cubic HYO. STEM image in Fig. 2(d) shows uniform growth of HYO on the MgO substrate. Complete mixing and uniform distribution of Y and Hf are shown in the energy dispersive spectroscopic (EDS) mapping in Figs. 2(e)–2(g). The cubic phase HYO found in our 20% Y:HfO_2 is in agreement with the results shown in the previous report on the crystal structures of bulk Y:HfO_2 with 20% Y doping concentration.[24]

For the HZO film, the thickness is found to be 145 ± 1 nm. The morphology of HZO films is drastically different in comparison to the HYO films. In Fig. 3(a), clear contrast between regions of different phases can be observed. The different crystal structures can be identified in magnified images in Figs. 3(b) and 3(d). The

TABLE I. Ionic radii of the metal cations in the studied material system.

Metal cations	Hf^{4+}	Y^{3+}	Zr^{4+}	Ce^{4+}	Ce^{3+}
Ionic radii (pm)	79 (Ref. 21)	101 (Ref. 22)	78 (Ref. 21)	111 (Ref. 23)	128.3 (Ref. 23)
Coordination number	8	6	8	8	6

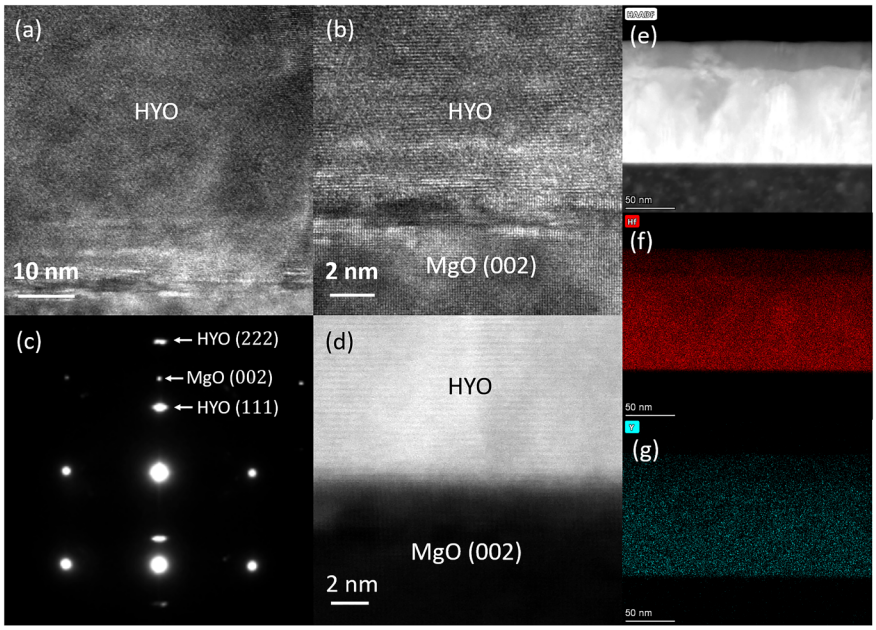

FIG. 2. Structural characterization of the HYO (20 mol. % Y: HfO_2) film on the MgO (002) substrate. (a) TEM image of the cubic phase HYO, (b) HRTEM of the HYO/MgO interface, showing the cubic phase HYO and cubic MgO. (c) Selected area electron diffraction (SAED) of the HYO film on the MgO substrate. (d) STEM image of HYO/MgO. (e)–(g) HAADF image of the film and EDS mapping of Hf and Y.

HZO films are predominantly in the monoclinic phase, in contrast to HYO, with inclusions of the cubic phase. Electron diffraction in Fig. 3(c) shows the presence of multiple sets of diffraction patterns suggesting the incorporation of multiple phases and different orientations in the film. Complete mixing and uniform distribution of Hf and Zr are shown in the energy dispersive spectroscopic (EDS) mapping in Figs. 3(e)–3(g).

For the HCO film, the thickness is found to be 69 ± 0.7 nm. Two different crystal structures, cubic and monoclinic, are observed in the TEM and STEM images, as shown in Figs. 4(a), 4(b), and 4(d). Electron diffraction shown in Fig. 4(c) confirms the presence of monoclinic phase grains with mirrored orientations. The presence of monoclinic and cubic phase is in agreement with previous reports of HCO films for large crystallite sizes and with

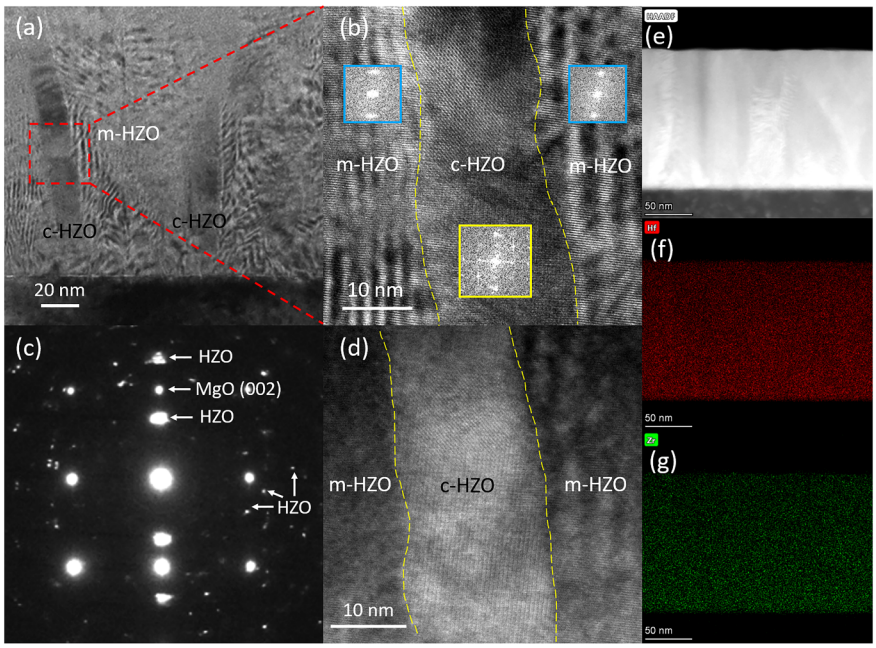

FIG. 3. Structural characterization of $Hf_{0.5}Zr_{0.5}O_2$ (HZO) on the MgO (001) substrate. (a) TEM image of the HZO film on the MgO (001), showing domains of monoclinic HZO (m-HZO) and cubic HZO (c-HZO). (b) TEM image of the enclosed region from (a) alternating m-HZO and c-HZO with clear phase boundaries are shown. Insets are the local fast Fourier transformation (FFT) of monoclinic and cubic HZO, respectively. (c) Selected area electron diffraction (SAED) of the HZO film on the MgO substrate. (d) STEM image of the enclosed region from (a). (e)–(g) HAADF image of the film and EDS mapping of Hf and Zr.

no/little concentration Ce^{3+} (Refs. 25–27). EDS mapping of the HCO film shown in Figs. 4(e)–4(g) also suggests complete mixing of Hf and Ce.

We now move onto the optical characterization of HYO, HZO, and HCO films and later discuss the results with regards to structural characterization and dopant properties. A J. A. Woollam VASE ellipsometer was used to measure the perpendicular (R_s) and parallel (R_p) (with respect to the plane of incidence) reflection coefficients of the sample in the range from 300 to 2000 nm. The ratio of these reflection coefficients defines the two parameters, Ψ and Δ, at a given wavelength and incidence angle, by Eq. (1),

$$\rho = \frac{R_p}{R_s} = \tan(\Psi) e^{i\Delta}. \quad (1)$$

Ψ and Δ data are shown in Figs. 5(a)–5(c) in red and green lines at 5 different incident angles (30°, 40°, 50°, 60°, 70°), respectively. The results of the corresponding Ψ and Δ are fitted with a mathematical model consisting of a B-spline bi-axial layer for film simulation and a MgO substrate from the J. A. Woollam's material library. The fits match the raw data with a mean-square error (MSE) around 5, indicating that the fitting model is properly selected. Thicknesses obtained from the fitting results are 97.68, 116.79, and 69.54 nm for HYO, HZO, and HCO, respectively, are in good agreement with the thicknesses derived directly from TEM and STEM images. This fitting results offer a reference for future (*in situ*) thickness estimation of HfO_2-based compounds using optical characterization. The permittivity results (real part ε_r and imaginary part ε_i), shown in Fig. 5(d), are derived by fitting the ellipsometric Ψ and Δ data using the general oscillator (Gen-Osc) model to enforce the Kronig consistency, which ensures the realistic shape of the optical dispersion.

The lowest real permittivity is observed in the HYO films, with dispersion from 5.07 at 300 nm to 4.27 at 2000 nm. An intermediate real permittivity is found in the HZO film, where the value of permittivity varies from 5.39 at 300 nm to 4.33 at 2000 nm. The feature found at around 500 nm in HZO film is associated with the increase in absorption loss potentially due to the interaction between the incident beam and vertical phases and grains in the HZO sample. HCO film shows the highest real permittivity with the largest dispersion from 7.66 at 300 nm to 4.71 at 2000 nm. The refractive index n and extinction coefficient k are directly related to the real part of the dielectric permittivity (ε_r) by the following equation: $\varepsilon_r = n^2 - k^2$. For transparent oxide thin films, the

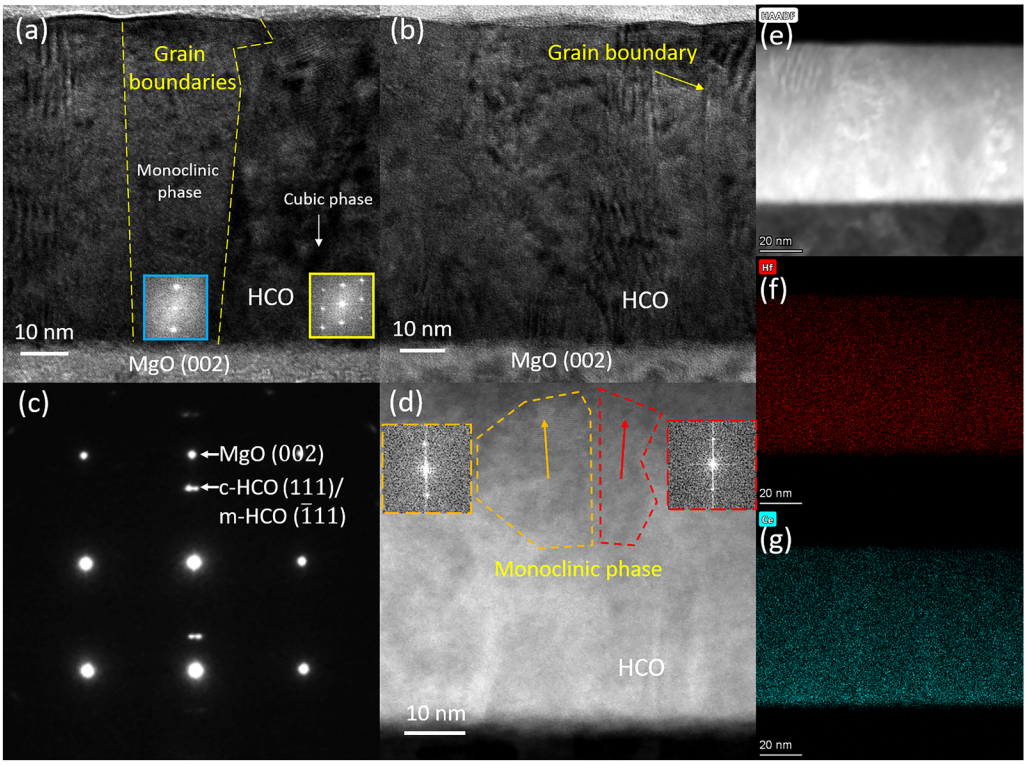

FIG. 4. Structural characterization of $Hf_{0.5}Ce_{0.5}O_2$ (HCO) on the MgO (001) substrate. (a) TEM image of the HCO film on the MgO (001). Clear grain boundaries between the monoclinic and cubic phase HCO are shown. Insets are the local fast Fourier transformation (FFT) of monoclinic and cubic HCO, respectively. (b) TEM image of HCO on the MgO substrate. (c) Selected area electron diffraction (SAED) of the HCO film on the MgO (001) substrate. (d) STEM image of the HCO film, domains of the monoclinic phase HCO with mirrored orientations are marked out by dashed lines. Insets show the corresponding local FFT of the two domains. (e)–(g) HAADF image of the film and EDS mapping of Hf and Ce.

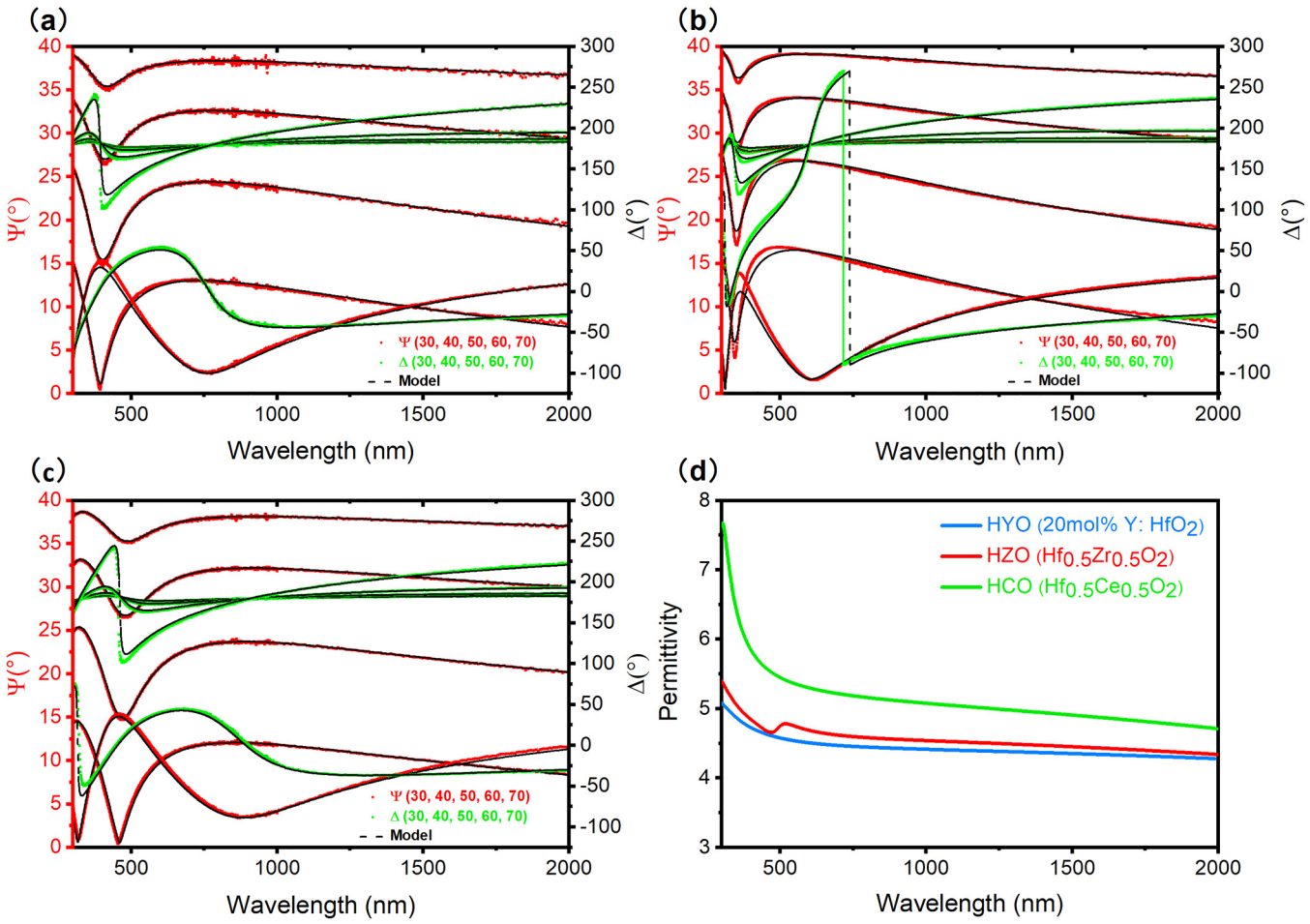

FIG. 5. Ellipsometry data and real permittivity of HYO (20 mol. % Y: HfO_2), HZO ($Hf_{0.5}Zr_{0.5}O_2$), HCO ($Hf_{0.5}Ce_{0.5}O_2$). (a)–(c) Reflectance data measured at five different incident angles (30°, 40°, 50°, 60°, 70°) for all three samples (HYO, HZO, and HCO). Black dashed lines represent the fitting results of Ψ and Δ using a B-spline model. (d) Real part of the permittivity of all three samples, extracted from the ellipsometry data using the general-oscillator (Gen-Osc) model.

extinction coefficient k is usually several orders of magnitude smaller than n. Thus, the real dielectric permittivity ε_r can be estimated by the value of n by $\varepsilon_r \approx n^2$. We thus estimate the refractive indices in the measured wavelength range (300–2000 nm) to be 2.25–2.07, 2.32–2.08, 2.77–2.17, for HYO, HZO, and HCO, respectively.

IV. DISCUSSION

We relate the optical properties (relative permittivity) of our films to their crystal structure and dopant materials. Relative permittivity of a system depends on its molar polarizability and molar volume, which are determined by the composition, phase, and crystallinity (density).[31] Properties of thin films additionally depend on the growth parameters, substrate, thickness, etc., For a solid solution, relative permittivity can be approximated by a weighted average of the relative permittivities of the two constituent materials in the simplest scenario. An addition of a dopant material can, however, provoke phase changes in the host material resulting in a drastically different relative permittivity than the equilibrium phase of the host. In the case of phase change upon doping, it is difficult to disentangle the effects of (1) mixing of two materials with different relative permittivities and (2) phase change upon doping, on the relative permittivity of the final material. We thus compare the trend of the measured refractive indices with the expected trends depending on the crystal structure and the dopant material. To interpret the fitting results, we consider previous studies on the value of refractive index in HfO_2 and corresponding dopants. We summarize the comparison for refractive index at 600 nm in Table II.

In experimental studies of HfO_2 films in the monoclinic phase, refractive index of 2.38–2.12 (Ref. 23) and 2.2–2.1 (Ref. 22)

TABLE II. Refractive indices *n* obtained at 600 nm wavelength of HYO, HZO, HCO films (monoclinic m, cubic c) compared to reported refractive indices of HfO_2 (experimental exp., *ab initio* ab in.) and dopants.

Films in this study	*n* (600 nm)	HfO_2	*n* (600 nm)	Dopants	*n* (600 nm)
c-HYO	2.12	m-HfO_2 (exp.)	2.2 (Ref. 22), 2.12 (Ref. 28)	c-Y_2O_3	1.93 (Ref. 29)
m/c-HZO	2.17	m-HfO_2 xx/zz (ab in.)	2.02/1.92 (Ref. 26)	m-ZrO_2	2.16 (Ref. 28)
c/m-HCO	2.30	c-HfO_2 (ab in.)	2.1 (Ref. 26)	c-CeO_2	2.32 (Ref. 30)

has been reported in the wavelength range of 300–2000 nm. The refractive index attributed to the electronic contributions has been calculated by Kumar *et al.*[32] in the wavelength range of 300–2000 nm to be 2.35/2.18–1.96/1.87 for the xx/zz components of the monoclinic phase and 2.54–2.02 for the cubic phase at 600 nm. In the case of mixed-phase samples, addition of cubic regions to a (nominally) monoclinic sample is expected to lead to an increase in the measured refractive index and more dispersion.

Furthermore, the refractive indices of dopants in the wavelength range of 300–2000 nm are 2.38–2.12 for HfO_2,[28] 2.0–1.8 for Y_2O_3,[29] 2.52–2.16 for ZrO_2,[28] and 2.8–2.2 for CeO_2.[30] It is expected that an intermediate refractive index value would be achieved in doped films according to the constituent compounds. The higher refractive index and more dispersion is observed in the films with dopants with higher refractive index and more dispersion.

Both the trend of the refractive index of constituent crystal structures and the refractive index of dopants match the trend of the refractive index observed in the corresponding films. Incorporating constituents with higher refractive indices can therefore tailor the refractive indices of the corresponding compounds effectively through crystal structure and electronic structure. In future studies, separating the contributions of crystal structure and dopants could be possible if one could control either of the parameters independently.

V. SUMMARY AND CONCLUSIONS

In summary, we compared the optical dielectric constant of HfO_2-based films of HYO, HZO, and HCO films on MgO substrates. We found that while the HYO film is stabilized in the cubic phase, the HZO films is stabilized in the monoclininc phase with partial incorporation of the cubic phase, and HCO is stabilized in the cubic phase with partial incorporation of the monoclinic phase. The optical permittivity of the films reveals the electronic contribution to the overall dielectric properties and a trend of higher permittivity for films with constituent phases and dopants of higher permittivity. Considering the significance of dielectric properties of HfO_2-based materials at optical frequencies, future directions should be centered around films grown on more prevalent substrates in the industry such as silicon,[33] which will provide crucial information for studies on the HfO_2-based devices for optoelectronic applications.

ACKNOWLEDGMENTS

The U.S.–U.K. collaborative effort was funded by the U.S. National Science Foundation No. ECCS-1902644 (Purdue University), No. ECCS-1902623 (University at Buffalo, SUNY)] and the EPRSC Grant No. EP/T012218/1. J.L.M.-D. and N.S. acknowledge support from the Swiss National Science Foundation under Project No. P2EZP2-199913 and the ERC Grant No. U-H2020-ERC-ADG No. 882929, EROS. J.L.M.-D. also acknowledges support from the Royal Academy of Engineering (Grant No. CIET1819_24).

AUTHOR DECLARATIONS

Conflict of Interest

The authors have no conflicts to disclose.

DATA AVAILABILITY

The data that support the findings of this study are available from the corresponding author upon reasonable request.

REFERENCES

[1]M. Muroi, M. Hagiwara, and S. Fujihara, ECS J. Solid State Sci. Technol. **8**, R169 (2019).
[2]M. Vargas, N. R. Murphy, and C. V. Ramana, Appl. Phys. Lett. **104**, 101907 (2014).
[3]S. Duenas, H. Castan, H. Garcia, and L. Bailo, *Dielectric Material* (InTech, 2012), pp. 213–249.
[4]J. Robertson, J. Vac. Sci. Technol. B **18**, 1785 (2000).
[5]K.-L. Lin, T.-H. Hou, J. Shieh, J.-H. Lin, C.-T. Chou, and Y.-J. Lee, J. Appl. Phys. **109**, 084104 (2011).
[6]T. S. Böscke, J. Müller, D. Bräuhaus, U. Schröder, and U. Böttger, Appl. Phys. Lett. **99**, 102903 (2011).
[7]P. Gonon, M. Mougenot, C. Vallée, C. Jorel, V. Jousseaume, H. Grampeix, and F. El Kamel, J. Appl. Phys. **107**, 074507 (2010).
[8]M. H. Park, Y. H. Lee, T. Mikolajick, U. Schroeder, and C. S. Hwang, MRS Commun. **8**, 795 (2018).
[9]H. Mulaosmanovic, E. T. Breyer, S. Dünkel, S. Beyer, T. Mikolajick, and S. Slesazeck, Nanotechnology **32**, 502002 (2021).
[10]H. Dou, X. Gao, D. Zhang, S. Dhole, Z. Qi, B. Yang, M. N. Hasan, J. H. Seo, Q. Jia, M. Hellenbrand, J. L. MacManus-Driscoll, X. Zhang, and H. Wang, ACS Appl. Electron. Mater. **3**, 5278 (2021).
[11]D. L. Wood, K. Nassau, T. Y. Kometani, and D. L. Nash, Appl. Opt. **29**, 604 (1990).
[12]T. Shiraishi, S. Choi, T. Kiguchi, T. Shimizu, H. Funakubo, and T. J. Konno, Appl. Phys. Lett. **114**, 232902 (2019).
[13]S. J. Kim, J. Mohan, S. R. Summerfelt, and J. Kim, JOM **71**, 246 (2019).
[14]D. Tahir, S. K. Oh, H. J. Kang, and S. Tougaard, Thin Solid Films **616**, 425 (2016).
[15]J. Müller *et al.*, J. Appl. Phys. **110**, 114113 (2011).
[16]X. Wang, D. Zhou, S. Li, X. Liu, P. Zhao, N. Sun, F. Ali, and J. Wang, Ceram. Int. **44**, 13867 (2018).
[17]F. L. Martínez, M. Toledano-Luque, J. J. Gandía, J. Cárabe, W. Bohne, J. Röhrich, E. Strub, and I. Mártil, J. Phys. D: Appl. Phys. **40**, 5256 (2007).

[18]D. S. Jeong, H. B. Park, and C. S. Hwang, Appl. Phys. Lett. **86**, 072903 (2005).
[19]A. Wiatrowski, A. Obstarczyk, M. Mazur, D. Kaczmarek, and D. Wojcieszak, Coatings **9**, 106 (2019).
[20]I. C. Ho, Y. Xu, and J. D. Mackenzie, J. Sol-Gel Sci. Technol. **9**, 295 (1997).
[21]Group 4 - Zirconium and Hafnium, 3 Feb. 2021, available at https://chem.libretexts.org/@go/page/34479.
[22]D.-J. Kim, S.-H. Hyun, S.-G. Kim, and M. Yashima, J. Am. Ceram. Soc. **77**, 597 (1994).
[23]M. Winter, Webelements https://www.webelements.com (last accessed April 2022).
[24]X. Xu, F. T. Huang, Y. Qi, S. Singh, K. M. Rabe, D. Obeysekera, J. Yang, M. W. Chu, and S. W. Cheong, Nat. Mater. **20**, 826 (2021).
[25]M. Rothensteiner, A. Bonk, U. F. Vogt, H. Emerich, and J. A. Van Bokhoven, RSC Adv. **7**, 53797 (2017).
[26]L. M. Lopato and E. R. Andrievskaya, Powder Metall. Met. Ceram. **40**, 405 (2001).
[27]J. M. Raitano, S. Khalid, N. Marinkovic, and S. W. Chan, J. Alloys Compd. **644**, 996 (2015).
[28]W. T. Tang, Z. F. Ying, Z. G. Hu, W. W. Li, J. Sun, N. Xu, and J. D. Wu, Thin Solid Films **518**, 5442 (2010).
[29]T. Wiktorczyk, P. Biegański, and J. Serafińczuk, Opt. Mater. **59**, 150 (2016).
[30]F.-C. Chiu and C.-M. Lai, J. Phys. D: Appl. Phys. **43**, 075104 (2010).
[31]S. Chen, Z. Liu, L. Feng, and X. Che, J. Mater. Sci. Mater. Electron. **25**, 749 (2014).
[32]M. Kumar, R. P. Singh, and A. Kumar, Optik (Stuttg) **226**, 165937 (2021).
[33]L. Sun, J. G. Jones, J. T. Grant, N. R. Murphy, C. V. Ramana, K. G. Eyink, J. P. Vernon, and P. R. Stevenson, ACS Appl. Nano Mater. **4**, 10836 (2021).